PLANETARY SCIENCE

A compositionally heterogeneous martian mantle due to late accretion

Simone Marchi[1]*, Richard J. Walker[2], Robin M. Canup[1]

The approximately chondritic estimated relative abundances of highly siderophile elements (HSE) in the bulk martian mantle suggest that these elements were added after Mars' core formed. The shergottite-nakhlite-chassigny (SNC) meteorites imply an average mantle Pt abundance of ≈3 to 5 parts per billion, which requires the addition of 1.6×10^{21} kilograms of chondritic material, or 0.25% martian masses, to the silicate Mars. Here, we present smoothed particle hydro-dynamics impact simulations that show that Mars' HSE abundances imply one to three late collisions by large differentiated projectiles. We show that these collisions would produce a compositionally heterogeneous martian mantle. Based mainly on W isotopes, it has been argued that Mars grew rapidly in only about 2 to 4 million years (Ma). However, we find that impact generation of mantle domains with variably fractionated Hf/W and diverse ^{182}W could imply a Mars formation time scale up to 15 Ma.

INTRODUCTION

The late accreted mass required to account for Mars' highly siderophile element (HSE) abundances may have been supplied by a very small number of large projectiles. In the standard assumption that all of a projectile's HSE were retained in the martian mantle, a single bulk chondritic projectile with $D \approx 10^3$ km could suffice, assuming a projectile density of 3000 kg/m^3 (Materials and Methods) (*1*–*3*). At least one impact of this scale is needed to account for Mars' largest putative preserved crater, the 10,600 × 8500 km Borealis basin (*4*, *5*).

Large projectiles ($D > 500$ km) are likely to have been differentiated (*6*), with most of their siderophile elements sequestered in their metallic cores. A large projectile's core may not be efficiently dispersed within the target's mantle during a collision (*6*, *7*). Hence, large projectiles may lead to a nonchondritic and initially nonuniform distribution of HSE in the martian mantle. The presence of ^{182}W (and ^{142}Nd) isotopic heterogeneities in martian meteorites (*8*) indicates that convection did not homogenize the early martian mantle, which is consistent with interior models (*9*–*11*). Thus, chemical and isotopic heterogeneities in the martian mantle created during late collisions may have been preserved and be reflected in the siderophile abundances and ^{182}W isotopic compositions of the shergottite-nakhlite-chassigny (SNC) meteorites (*12*, *13*).

RESULTS

To investigate mixing of material from late, large projectiles into Mars, we performed smoothed particle hydrodynamics (SPHs) simulations with 0.5×10^6 to 1.2×10^6 particles for two projectile masses, M = 0.003 and $0.03M_m$ (where M_m is Mars' mass), with impact angles β = 0°, 30°, 45°, and 60°, and impact velocities (v) of v/v_e = 1.5, 2, and 2.5 (where v_e is the mutual escape velocity). These mass and velocity ranges encompass those inferred for the Borealis basin (*4*, *5*) and predicted by dynamical models of late accretion (*14*). Our projectiles have metallic cores comprising 30% of their mass and are resolved by 10^3 to 10^4 SPH particles. Our simulations neglect material strength. This is a good approximation for early Mars because its mantle temperature would have been near the solidus (*10*), and overburden pressure due to gravity would have exceeded shear strength in its warm mantle (Materials and Methods). Furthermore, at impact velocities we consider (7 to 12 km/s), projectile material is melted by the impact, and so, strength can also be neglected in modeling its evolution (Materials and Methods).

In a large collision, substantial portions of the projectile's core merge with Mars' core, and only part is retained within Mars' mantle (Fig. 1; Materials and Methods), in keeping with previous results for large terrestrial impacts (*6*). For $M = 0.003M_m$ (=1.9×10^{21} kg; $D \approx$ 1000 km) and a typical impact speed $v/v_e = 2$ (*10*), we estimate that ≈20% of a projectile's core is retained in the martian mantle when averaging over impact angles (Materials and Methods), with this percentage varying from 0 to 45% across all β and v/v_e. The angle-averaged value implies that about four such projectiles with a total mass of $\approx 7 \times 10^{21}$ to 8×10^{21} kg would be required to deliver the mantle HSE budget of Mars. For $M = 0.03M_m$ (= 19×10^{21} kg, $D \approx$ 2100 km), the maximum retention is 17% across all β and v/v_e. Thus, a single $0.03M_m$ projectile could deliver all the martian mantle HSE. A projectile diameter $D \approx$ 700 to 2700 km is thought responsible for Borealis (*4*, *5*). Smaller projectiles are estimated for Mars' next largest Utopia and Hellas basins ($D \approx$ 300 to 800 km) (*15*), and these may account for less than 10% of Mars' HSE (*2*). If supplied by a single oblique collision, Mars' spin implies a $\approx 0.03M_m$ mass projectile ($D \approx$ 2000 km) (*16*). Together, the above estimates suggest that Borealis could be due to one of the largest late accretion projectiles, with up to about three unpreserved, comparably or larger sized events occurring before its formation.

To explore the effects of heterogeneous projectile mixing during late accretion, we compute the ratio of projectile material to martian mantle material within conic domains with a semi-aperture angle of 30°, each corresponding to about 7 volume % of the mantle. With this choice, a single domain typically contains the predominant effects of each collision (Materials and Methods). We then calculate the effects such additions would have on the initial mantle concentrations of Pt, W, and Hf/W in these domains. Platinum is typically not strongly fractionated between mantle sources and basaltic crust [e.g., (*12*)], so while SNC meteorites sample martian crust, their Pt concentrations can serve as a general proxy for HSE concentrations in the mantle sources of these rocks.

[1]Southwest Research Institute, Boulder, CO, USA. [2]Department of Geology, University of Maryland, College Park, MD, USA.
*Corresponding author. Email: marchi@boulder.swri.edu

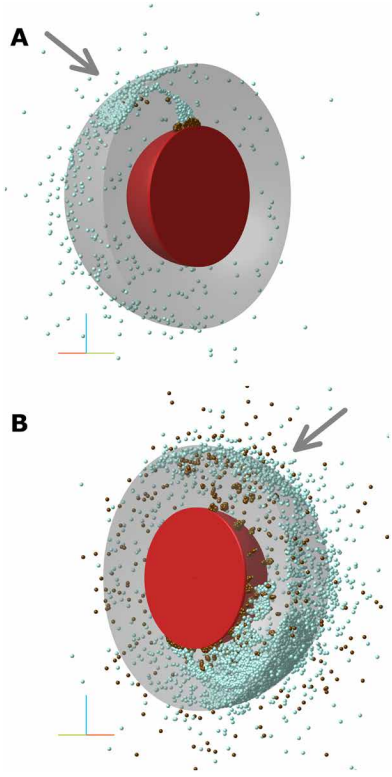

Fig. 1. Heterogeneous projectile mixing in martian mantle. End state of two representative high-resolution SPH simulations (1.2×10^6 particles). (**A**) $M/M_m = 0.003$, $v/v_e = 2$, $\beta = 30°$. (**B**) $M/M_m = 0.03$, $v/v_e = 2$, $\beta = 45°$. In both cases, martian particles are not shown for clarity, while red and gray half-spheres schematically indicate martian core and mantle, respectively. Projectile's core and mantle particles are indicated by brown and green spheres, respectively. The arrows indicate local concentration of projectile mantle (A) and core (B) materials. Preimpact SPH particles have a characteristic smoothing length of ≈50 to 60 km. The orientation vectors are shown at the bottom left corner of each panel: *x* axis (red), *y* axis (blue), and *z* axis (green).

For a $0.03M_m$ collision, the projectile core to martian mantle ratio varies from 0 to 0.008 in the conic domains around the whole planet, resulting in Pt concentrations that range from 0 (exclusively the Pt residual from primary core separation) to 25 parts per billion (ppb) (Materials and Methods). For a $0.003M_m$ projectile, Pt domain concentrations range from 0 to 13 ppb. Considering up to four such impacts, the mantle Pt concentration could locally vary from 0 to a maximum allowable ≈50 ppb (i.e., 13 ppb × 4 impactors). If the martian mantle was not well mixed, SNC meteorites with average abundances of Pt ≈ 3 to 5 ppb might not be representative of the bulk mantle but could instead reflect local HSE heterogeneities. SNC meteorites display a considerable variation in Pt concentrations: e.g., shergottite Y980459 has ≈20 ppb Pt, while Dhofar 019 has 0.071 ppb Pt (*12*). This provides strong evidence that mantle HSE abundances are nonuniform. Addition of projectile core material to a mantle domain without substantial subsequent mixing could account for high concentrations (e.g., Y980459), while limited incorporation of projectile core or projectile mantle materials in other regions could account for low concentrations, e.g., Dhofar 019. The SNC meteorites reflect material melted long after late accretion, and their source region(s) is unknown. The best candidate locations for some shergotty- and chassigny-like meteorites, based on remote spectral measurements, are found in proximity of the Borealis' rim (*17*). These SNC compositions might reflect heterogeneous mixing of the Borealis' projectile into the mantle and preservation through the early formation of a stagnant, near-surface layer (*18*).

Heterogeneous projectile mixing may also have influenced the radiogenic isotope systems used to probe internal processes in the martian mantle (e.g., magma ocean fractionation) or to constrain the formation time of Mars. Of particular interest are the short-lived ^{182}Hf-^{182}W [^{182}Hf → ^{182}W + 2β$^-$, half-life ($T_{1/2}$) = 8.9 million years (Ma)] and ^{146}Sm-^{142}Nd (^{146}Sm → ^{142}Nd + α, $T_{1/2}$ = 103 Ma) systems, whose isotopic compositions are normally reported as the ratios of ^{182}W to the stable and nonradiogenic ^{184}W, and ^{142}Nd to the stable and nonradiogenic ^{144}Nd. Compositions can be expressed as the parts per 10,000 deviation in these ratios relative to a reference bulk silicate Earth (BSE) ratio estimate [e.g., $\varepsilon^{182}W = 10^4 \times \{(^{182}W/^{184}W)/(^{182}W/^{184}W)_{BSE} - 1\}$]. Variations in ε^{182}W values can reflect metal-silicate segregation, while ^{182}Hf was extant in the first 60 Ma of solar system history, given the lithophile and siderophile natures of Hf and W, respectively [e.g., (*19*)]. Silicate crystal-liquid fractionation processes during the same time period can also lead to changes in ε^{182}W values, given the more highly incompatible nature of W relative to Hf. The ε^{182}W value in a planetary mantle or crust domain can also be modified by the addition of separately formed projectiles. By contrast, ε^{142}Nd values are primarily affected by silicate crystal-liquid fractionation processes during the first 600 Ma of solar system history and would be minimally affected by either core segregation or late accretion, given that both parent and daughter elements are strongly lithophile. Foley *et al.* (*20*) and Kruijer *et al.* (*13*) noted a broad positive correlation between ^{182}W and ^{142}Nd for SNC meteorites, with ε^{142}Nd values for the martian meteorites, for which ε^{182}W values have been reported, ranging from −0.45 (NWA 7034) to +0.92 (NWA 7635), while ε^{182}W values range from +0.20 to +1.80, respectively, for the same meteorites. Variability in ε^{182}W and ε^{142}Nd values for martian meteorites has been ascribed to a combination of core formational (for W) and silicate crystal-liquid fractionation processes (for W and Nd) (*13*, *20*). The general positive correlation between ε^{182}W and ε^{142}Nd suggests the involvement of early magma ocean silicate fractionation processes in the establishment of heterogeneity of short-lived radiogenic isotope systems. However, there is considerable variation about the linear trend that would not be expected to result from single-stage magma ocean crystallization. Delivery of mantle/core material by sizable impactors would have been associated with substantial but nonglobal melting of the mantle (fig. S1). One or more such impacts may have provided the venue for the proposed large-scale silicate-silicate fractionation (*13*, *20*) to account for the ^{182}W-^{142}Nd correlation observed in data for SNC meteorites. The broad positive correlation is consistent with a fractionation event and subsequent mixing 20 to 25 Ma after solar system formation (*13*). The correlation is characterized by much less scatter than the ^{182}W-^{142}Nd trend, consistent with additional processes, such as late accretion, creating ^{182}W isotopic variations that were unrelated to silicate-silicate fractionation. Here, we propose that the uneven delivery of mantle and core materials to the melted domains could have led to the superimposition of these effects on top of the effects resulting from silicate-silicate fractionation.

Heterogeneous delivery of projectile material to the martian mantle can result in localized positive or negative ε^{182}W anomalies, depending on the proportion of projectile mantle (with high Hf/W and high ^{182}W due to earlier core formation within the smaller projectile) versus core (with low Hf/W and low ^{182}W) added to the domain.

To quantify this, we track the combined evolution of HSE (using Pt as a proxy) and Hf-W concentrations, as well as ε^{182}W values, in martian mantle domains resulting from a small number of collisions. Projectiles and Mars are assumed to have bulk chondritic HSE and ε^{182}W compositions (present-day ε^{182}W = −1.9) and to have single-stage core formations (instantaneous differentiation into core and mantle) at 2 and 3.5 Ma, respectively. We implement a Monte Carlo approach to track the time evolution of ε^{182}W in conic domains randomly located on the planet in 400 simulations in which collisions occur randomly throughout a 10- to 15-Ma to 100-Ma timeframe (Materials and Methods).

Figure 2A shows the results for a late accretion involving three collisions (see Materials and Methods for additional examples). For simplicity, we assume that only one collision in each timeline delivers a significant projectile core material to the martian mantle. For this collision, we randomly select the mass ratio of projectile core to Mars mantle from 0.0004 to 0.008, the latter being the maximum concentration inferred from our SPH simulations in a conic domain. The other two collisions deliver projectile mantle to the same conic domain with a random mixing ratio from 0 to 0.7, as bound by our SPH simulations (Materials and Methods). With these assumptions, the final Pt concentrations range from ≈1 to 20 ppb, broadly compatible with meteorite observations. Hf-W models track ^{182}W growth until ^{182}Hf extinction. The final ε^{182}W values in our simulations range from +0.60 to +6.00 (Fig. 2A). For comparison, SNC meteorites exhibit variations in ε^{182}W values in pyroxenites from ≈+0.09 (orthopyroxene-rich martian meteorite ALH 84001) to +3.35 (nakhlite NWA 998) (Fig. 2A) (*8*, *13*, *20*). Shergottites are only slightly less heterogeneous, with values ranging from +0.29 (intermediate shergottite EETA 79001 lithology B) to +1.80 (depleted shergottite NWA 7635) (*13*). By comparison, the total reported range in ε^{182}W for terrestrial rocks is substantially smaller, ≈−0.20 to +0.49 (*21*–*24*). Late accretion, as envisioned here, has the potential to strongly modify ^{182}W isotopic heterogeneity originally produced by silicate fractionation. We note that the results of our model do not strongly depend on the assumed input parameters, such as the cone semi-aperture angle. Last, the assumed mixing of either projectile's core or mantle material from different collisions is quantitatively similar to mixing of both components in every collision; thus, other mixing scenarios are also possible.

For completeness, we also investigate final ε^{182}W and Pt values for representative Monte Carlo mixing calculations based on a three-collision scenario (as in Fig. 2B). We find that ε^{182}W is largely decoupled from the final concentration of Pt. The delivery of projectile core in one collision (as we have assumed in our simulations) largely sets the final Pt content, while variable amounts of added projectile mantle by the two other collisions can produce large variations in the final ε^{182}W, with only a minor effect on Pt (Materials and Methods). We discuss the effect of heterogeneous projectile accretion on other isotopic system, such as oxygen, in Materials and Methods.

An inferred single-stage core Hf-W formation age of 3.5 Ma for Mars is based on an estimated value of ε^{182}W = +0.37, approximately the average for shergottite meteorites, coupled with an average ^{180}Hf/^{184}W of 4.0 extrapolated from Th/W ratios for shergottites (*19*). An alternative model based on continuous accretion estimates that Mars reached 44% of its mass in ≈1.8 Ma (*25*). These calculations assume that shergottites are representative of the bulk silicate Mars. However, these estimated core formation ages would be incorrect if the ε^{182}W value for pre-late accretion bulk silicate Mars ($\varepsilon^{182}W_{pre}$) is either higher or lower than previously assumed due to incomplete projectile mixing effects. Higher ε^{182}W values, as might be indicated by some nakhlites and shergottite values >+1.0, would imply an even earlier formation age. Alternatively, if ALH 84001 (ε^{182}W = +0.09)

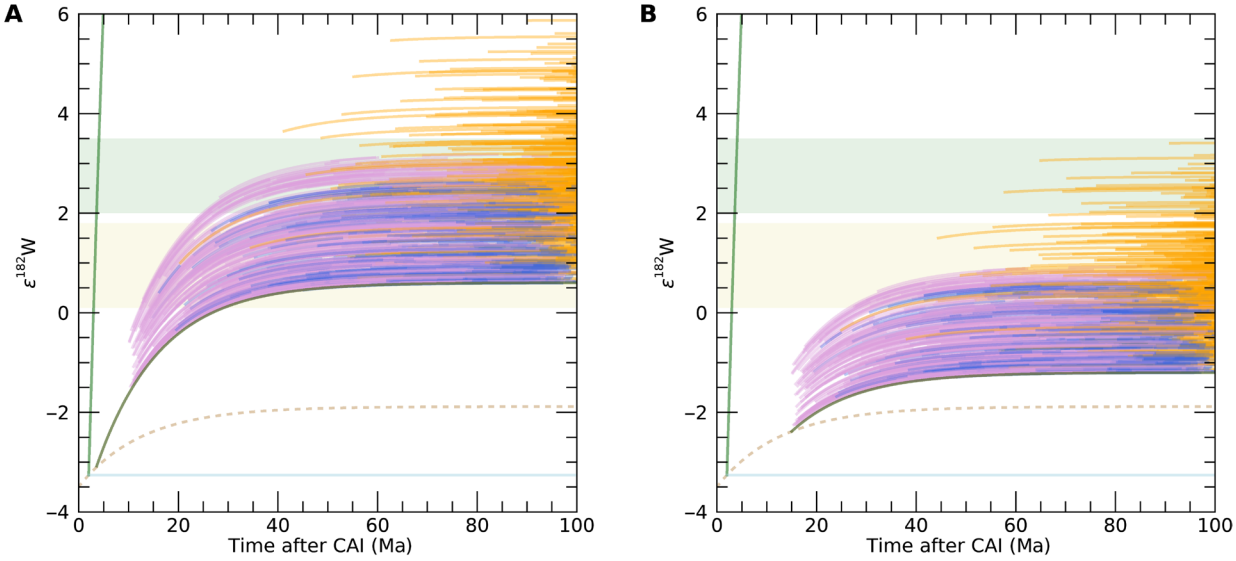

Fig. 2. Hf-W isotopic evolution of early Mars. The time evolution of ε^{182}W in early mantle domains that have received mantle and core materials from three projectiles. Time is after the condensation of the first solar system solids [calcium-aluminum-rich inclusions (CAI)]. The brown dashed line indicates the evolution of an undifferentiated chondritic body. Divergent light green and blue lines at 2 Ma indicate the evolution of projectile mantle and core, respectively. Dark green lines starting at 3.5 (**A**) and 15 Ma (**B**) indicate the evolution of the prelate accretion mantle of Mars. These curves are chosen to give a final prelate accretion $\varepsilon^{182}W_{pre}$ ≈ +0.6 [(A); appropriate for an early-formed Mars as assumed previously] and −1.2 [(B); appropriate for a late-formed Mars at 15 Ma]. Collisions take place randomly between 10 to 100 Ma and 15 to 100 Ma for (A) and (B), respectively. Violet, blue, and orange segments indicate the evolution of mantle domains after one, two, and three collisions, respectively. In this plot, we assume that the first and last collisions deliver projectile mantle, while the second collision delivers projectile core (see text and Materials and Methods for details). Each panel reports 400 random realizations. Horizontal shaded regions indicate the range of ε^{182}W observed in shergottites (yellow) and nakhlites (green).

is more representative of the bulk silicate Mars, then the model differentiation age would be considerably later.

To illustrate the effect of $\varepsilon^{182}W_{pre}$ on the formation age, we use a Monte Carlo code that randomly selects combinations of relevant parameters, including their uncertainties (Materials and Methods). The error analysis shows that a single-stage core formation age between 5 and 15 Ma requires $\varepsilon^{182}W_{pre}$ ranging from +0.1 to −1.2, respectively (Fig. 3). To investigate whether a much lower $\varepsilon^{182}W_{pre}$ value than previously assumed is compatible with SNC meteorites, we repeated the analysis with an extreme $\varepsilon^{182}W_{pre} = -1.2$. We find that the three-collision model can produce the observed range of HSE and $\varepsilon^{182}W$ values (Fig. 2B; Materials and Methods). Thus, our model shows that a formation age in excess of 5 Ma and as late as ≈15 Ma post-CAI (calcium-aluminum-rich inclusions) is possible. In this case, a solution with three projectiles is required to span the full range of observed SNC $\varepsilon^{182}W$ values.

DISCUSSION

The accretion history and formation time scale of Mars continue to be debated [e.g., (*26*)]. Recent terrestrial accretion models find that forming a fully grown Mars requires ≈10 Ma [e.g., (*27*)], consistent with constraints that require Mars' crust to have formed within the first 20 Ma of solar system history (*13*, *28*). Alternatively, formation models based on pebble accretion can grow Mars in a few million years (*29*); however, accretion histories in excess of 10 Ma are also commonly observed in those models. One way to reconcile a longer formation time scale with Hf-W constraints is to consider that Mars accreted via giant impacts (i.e., by bodies containing 10% or more of its mass) whose cores did not efficiently equilibrate with its mantle [e.g., (*30*)]. However, Mars' small mass and its slow rotation rate seem to imply that it is a leftover planetary embryo that formed primarily through accretion of smaller bodies. Our heterogeneous mixing model shows that late accretion by just a few projectiles of mass $10^{-3}M_m$ to $10^{-2}M_m$ provides a way to reconcile Mars' formation as an embryo with the protracted growth time scale predicted by some accretion models. The time scale for the dispersal of the solar protoplanetary disk is estimated to be ≈4 to 5 Ma, based on paleomagnetic measurements in angrite meteorites (*31*) and Pb-Pb ages of chondrules in a CB meteorite (*32*). Late formation would imply that Mars completed its growth in a gas-poor/gas-free environment, in contrast to previous estimates that suggest that Mars formed while the Sun's full gaseous protoplanetary disk was likely still present (*25*), with implications for the mode of Mars' growth, its post-accretion thermal state, and the acquisition of its early atmosphere.

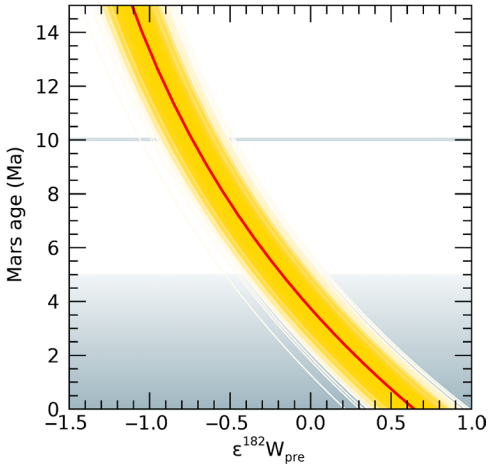

Fig. 3. Mars formation time scale. Nominal formation age as a function of pre-late accretion mantle $\varepsilon^{182}W_{pre}$. The red curve corresponds to the nominal model that uses average values for the input parameters (see text). The yellow envelope indicates 2×10^3 Monte Carlo draws to encapsulate uncertainties in the model age (Materials and Methods). Gray shaded region indicates formation ages below 5 Ma, an upper limit for the dissipation of the solar protoplanetary disk (see text). For reference, the horizontal line at 10 Ma marks the observed complete dissipation of protoplanetary disks around most stars. The lowest values for $\varepsilon^{182}W_{pre}$ (based on model 1-σ uncertainties) for 10 and 15 Ma are about −0.8 and −1.2, respectively (see text).

MATERIALS AND METHODS

Projectile mixing and late accreted mass

We use our SPH impact simulations to track the fate of the projectile core and define three end states: merges with Mars' core, remains suspended in the martian mantle, or ejected from the system (fig. S2). In doing this analysis, we follow the approach developed for the Earth (*6*).

Our martian simulations show that large, well-resolved clumps (>100 particles) of projectile's core typically reach the base of the core-mantle boundary (CMB) within 2 hours after contact. This rapid merger is driven by the direct excavation of the martian mantle by the projectile and deposition of projectile's core material at depth in the mantle (fig. S3). From this deposition location, projectile's core material descents to the CMB. The final descent through the mantle of these large core clumps is not likely to result in significant turbulent erosion because the vertical scale of the descent is comparable with the size of the clumps (*6*, *7*). Thus, this projectile's core material is not likely to isotopically or chemically equilibrate with the martian mantle. This rapid core descent is observed whenever a large clump of the projectile's core remains coherent. In collisions with high impact angles (≥45°), a part of the projectile's core is efficiently disrupted and is dispersed in the mantle or into the near surface (Fig. 1B and fig. S3B). The shearing associated with these oblique collisions results in a portion of the core being disrupted to single particles or small clumps. We assume that this material is retained in the mantle following the logic of Kendall and Melosh (*33*). This process is facilitated by the impact melting of significant volumes of the martian mantle, which would enhance turbulent erosion. In addition, note that our SPH technique may overestimate the final size of core particles that experience extreme shear conditions, which are typically achieved by stranded single particles (*34*). This facilitates equilibration, as smaller particles are prone to a more efficient turbulent erosion.

Notice that, in the study of Marchi *et al.* (*6*), we conducted a resolution test for 45° collisions in which the number of SPH particles in the projectile was varied by a factor of 25 across three simulations (from 2×10^2 to 6×10^3). The three runs yielded broadly similar large clump masses and a similar fraction of the impactor core that descends to the CMB. Here, we performed a similar test finding consistent results.

We investigate the post-collision concentration of projectile material in conic mantle domains located across the planet that have semi-apertures of 30°. With this definition, a single mantle domain often contains most of the localized effects of a collision. The choice of the semi-aperture angle does not significantly alter the overall

results. Over the assumed range of projectile masses and velocities and for an average impact angle of 45°, we find that the ratio of projectile core to Mars' mantle varies from 0 to 0.008 (see the main text and Fig. 1B), depending on the domain location with respect to the impact geometry. For impact angles less than 30° (not shown in fig. S2 for clarity), the projectiles' core and mantle effectively separate: The core merges with the martian core, while the impactor mantle is mostly deposited close to the martian surface (Fig. 1A). For the domain with the greatest concentration of projectile mantle material, we find that in a 200-km-thick surface spherical cap with a semi-aperture of 30°, the ratio of projectile mantle to Mars' mantle ranges from 0 to 0.7 across the investigated range of projectile masses and velocities, similar to that found for impacts into Earth (*6*). These mixing ratios are used in our Monte Carlo mixing simulation to track Pt and Hf-W evolutions (Fig. 2).

Our SPH simulations neglect material strength. This is a good approximation for large targets when the overburden pressure due to gravity, ρgh (where ρ is the density, g is the gravitational acceleration, and h is the depth), exceeds the shear strength (*35*). The largest shear strength for dunite or basalt occurs for high pressures and low temperatures, and is ≈3.5 GPa (*36*). The overburden pressure within Mars exceeds this value for depths greater than about 270 km (*37*), increasing to about 20 GPa at the CMB. Thus, for low temperatures, strength can be neglected in the inner martian mantle but could be important in outer mantle regions. Recent SPH impact simulations (*38*) that incorporate a strength model (*35*) found that strength had a significant effect on the distribution of projectile mixing within a martian mantle whose CMB temperature was T_{CMB} = 1500 K. This is a "low-temperature" Mars in the sense that it is much cooler that the solidus temperature, which at the CMB is $T_{s,CMB}$ ≈ 2500 K (*39*).

However, at the time of late accretion, early Mars' interior was likely substantially hotter and closer to the solidus, with T_{CMB} ≈ 2200 to 2400 K estimated from interior models [(*10*); their figure 3A]. As temperatures approach the liquidus, materials soften and weaken, which reduces strength by an approximate factor $\tanh[1.2(T_l/T - 1)]$ (where T_l is the local liquidus temperature and T is the material temperature), with strength effectively vanishing once $T = T_l$ (*35*, *38*, *40*). For temperatures expected during late accretion (i.e., T_{CMB} ≈ 2200 to 2400 K), this temperature-dependent softening would reduce strength by a factor of several to >10 in the martian mantle relative to that considered by Emsenhuber *et al.* (*38*), who assumed a cooler profile with T_{CMB} = 1500 K. For shear strengths ≤1 GPa, overburden pressure would exceed strength for depths greater than 10^2 km. Thus, all depths within an early warm Mars that are resolved by our SPH simulations (whose individual particle diameters are 10^2 km) are well approximated by a strengthless model.

Projectile material has much lower initial overburden pressures but is heated by the impact. We consider impact velocities between ≈7 and 12 km/s, based on numerical simulations of late accretion (*14*), so that the impact energy is ≈2×10^{11} to 7×10^{11} erg per unit mass of the projectile. Typically, a few percent of the initial impact energy is partitioned into heating the projectile material, e.g., figure 5.5 in (*41*), which, for our impact velocities, implies that the projectile is heated by ≈7×10^9 to 2×10^{10} erg/g, substantially exceeding the latent heat of fusion (≈2×10^9 to 3×10^9 erg/g) for mantle and core materials. Thus, projectile mantle and core retained within the martian mantle in our simulations is shock-heated to or beyond the melting temperature and strength within this material will be unimportant. In addition, iron meteorites provide a direct constraint on the crystallization time of their parent bodies (200 to 500 km in size), which can be up to a few tens of millions years (*42*). It is therefore anticipated that the cores of larger planetesimals, such as those considered in our work, could have been molten for a longer time scale, comparable or longer than the time scale in which most collisions take place in our model. We note that this may not have been the case in the simulations of Emsenhuber *et al.* (*38*), which considered a very low impact velocity of 4 km/s (less than the ≈4.5 km/s mutual escape velocity we estimate for their collision setup) and an impact energy per unit projectile mass of just 8×10^{10} erg/g, which is about three to nine times lower than in our simulations. At their low impact speed, heat retained in the projectile may have only been comparable to the latent of fusion, and so, it is possible that the projectile material within the martian mantle in their simulations had appreciable strength.

Pt and Hf-W mixing computations

For our computation, we assumed a starting bulk chondritic composition with Hf = 154 ppb, W = 133 ppb, $^{182}Hf/^{180}Hf = 1.02 \times 10^{-4}$, $^{182}W/^{184}W = 0.864477$, and Pt = 1100 ppb. This leads to a final $\varepsilon^{182}W = -1.89$ (Fig. 2). In the case of a homogeneous mixing of chondritic material to the bulk silicate mass (≈4.3×10^{23} kg) and a final average Pt ≈ 4 ppb (see the main text), the late accreted mass is ≈$4 \times 4.3 \times 10^{23}/1100 = 1.6 \times 10^{21}$ kg.

Differentiated projectiles are assumed to derive from chondritic objects that instantaneously differentiated at 2 Ma. The precise timing of differentiation does not significantly affect our results. We assume the following concentrations for the projectile mantle: Hf = 230 ppb, W = 6 ppb, and Pt = 0.1 ppb; and for the projectile core: Hf = 0 ppb, W = 397 ppb, and Pt = 3300 ppb. These values are consistent with the assumption of a chondritic bulk composition and a core with 33% of the total mass, which formed via metal-silicate equilibrium at low pressure (<1 GPa) and moderately low oxygen fugacity (IW-1), in which tungsten is moderately siderophile (D ≈ 30) (*43*). With these assumptions, the mantle and core acquire a final $\varepsilon^{182}W$ values of +42.3 and −3.26, respectively. We stress that the overall picture of our work is largely insensitive to the actual numerical values adopted above.

For a Mars assumed to have instantaneous differentiation at 3.5 Ma, we adopt a martian mantle with Hf = 222 ppb, W = 63.25 ppb, and Pt = 0.1 ppb. With these assumptions, we obtain a final $\varepsilon^{182}W_{pre} = +0.60$ (Fig. 2A and fig. S4A). In our Monte Carlo mixing calculations, we also consider a later Mars differentiation time of 10 Ma (with Hf = 222 ppb, W = 85 ppb, and Pt = 0.1 ppb) and 15 Ma (with Hf = 222 ppb, W = 81 ppb, and Pt = 0.1 ppb), resulting in a final $\varepsilon^{182}W_{pre} = -1.00$ and −1.20, respectively (Fig. 2B and fig. S4B). Details on the final $\varepsilon^{182}W$ and Pt values for our mixing model are reported in fig. S5.

Oxygen isotope mixing

Oxygen isotopes are often used to assess the composition of planets in relation to their building blocks, and they can also be useful to constraint the composition of late accreted materials. Here, we provide two examples. In the first case, we consider projectile's core mixing with the martian mantle. We used $\Delta^{17}O_p = 1.1$ and −0.7 for IVA and IAB iron meteorites, respectively. The $\Delta^{17}O_{mix}$ of the mix is

$$\Delta^{17}O_{mix} = X_p \times \Delta^{17}O_p + X_{mars} \times \Delta^{17}O_{mars}$$

where X_p and X_{mars} are the fraction of both components in a mantle domain ($X_p + X_{mars} = 1$). From our SPH simulations, $X_p = 0.008$ at

most. We also take $\Delta^{17}O_{mars} = 0.3$ and obtain $\Delta^{17}O_{mix} = 0.306$ and 0.292 for IVA and IAB, respectively. Thus, core mixing has negligible effects on martian oxygen isotopes.

We now repeat the computation for projectile's silicate mixing with the martian mantle. For reference, we consider $\Delta^{17}O_p = -0.3$ typical of howardite-eucrite-diogenite meteorites. From our SPH simulations, X_p is up to 0.4 (notice that this is equivalent to the mass ratio of 0.7 discussed in the main text). Assuming $\Delta^{17}O_{mars} = 0.3$, we obtain $\Delta^{17}O_{mix} = 0.06$, which would be easily resolvable. We also compute that for a mass ratio X_p/X_{mars} below 15%, the effect of projectile mantle mixing on oxygen isotopes is negligible. However, our model does not consider or depend on the genetic characteristics of materials (which include oxygen isotopic compositions), and so, there is no a priori requirement that the late accreted materials would have substantially different oxygen isotopic compositions. Note that to some extent the uniformity of oxygen isotopic compositions in martian meteorites could be a self-fulfilling conclusion because oxygen isotopic compositions are a primary means of identifying martian meteorites.

The number of 1000-km versus smaller projectiles

The bombardment history of Mars has been the subject of two recent works. One model (*2*) argues that the Borealis impact happened very early in Mars history [≈4.5 billion years (Ga)] and that the observed number of large craters and basins is close to the actual number of collisions experienced by Mars since 4.5 Ga. An alternative model (*44*) envisions a much later formation for Borealis basin (≈4.3 Ga), associated with a global erasure of preexisting craters. The two models present very different collisional evolutions: few large collisions on Mars in the former versus many more large collisions in the latter. In model (*2*), most HSE are delivered by a Borealis-type impact, while in model (*44*), the large number of smaller projectiles could also contribute HSE. To test this possibility, we generated 500 Monte Carlo simulations with an input impactor size-frequency distribution (SFD) from Marchi *et al.* (*45*), with projectile sizes ranging from 12 to 4000 km. We selected simulations that gave one impactor ≥1000 km (one Borealis-scale event), as in model (*44*). Then, we integrated the impactor SFD to obtain the total mass colliding with Mars, excluding the largest Borealis impactor. This provides an estimate of the total mass delivered by sub–1000-km impactors. The mean total mass in 12- to 1000-km bodies was 5×10^{20} kg, assuming 100% accretion. This is significantly lower than the 1.6×10^{21} kg needed to explain Mars' mantle HSE in the limit that all projectile HSEs are retained in the martian mantle. Thus, even the most intense envisioned bombardment would not deliver Mars' HSE in only sub–1000-km projectiles. This is consistent with the idea that the HSE abundances in the martian mantle were primarily delivered by large (≥1000 km) projectiles.

Mars formation age

Under the simplified assumption of a single-stage differentiation and instantaneous Hf/W fractionation, the core formation age is given by

$$t = (1/\lambda) \ln(Q_w f/(\varepsilon^{182}W_{pre} - \varepsilon^{182}W_{chon}))$$

where $f = (^{180}Hf/^{184}W)_{pre}/(^{180}Hf/^{184}W)_{chon} - 1$. The assumed average values and 1-σ uncertainties are as follows: $\lambda = 0.078 \pm 0.002$, $(^{180}Hf/^{184}W)_{pre} = 3.51 \pm 0.45$, $(^{180}Hf/^{184}W)_{chon} = 1.35 \pm 0.11$, $\varepsilon^{182}W_{chon} = -1.9 \pm 0.1$, and $Q_w = 1.59$ is the difference between $\varepsilon^{182}W_{chon}$ and $\varepsilon^{182}W$ for the initial solar system (*19*, *25*). With these values, $\varepsilon^{182}W_{pre} = +0.45$ yields $t \approx 1$ Ma. This is comparable with a previous estimate ($t \approx 1.8$ Ma) based on a continuous accretion model (*25*). For reference, the same approach yields a formation age of ≈34 Ma for Earth (*19*).

As noted above, in our model, we have a pre-late accretion $\varepsilon^{182}W_{pre} \approx +0.6$ (Fig. 2A). However, as discussed in the main text, heterogeneous projectile mixing can result in a strong nonchondritic $\varepsilon^{182}W$ addition to mantle domains. To investigate the effect of $\varepsilon^{182}W_{pre}$ on the formation age, we run a Monte Carlo code that randomly selects 2×10^3 combinations of the individual parameters each chosen from a Gaussian distribution with the specified average and 1-σ values. The error analysis shows that a formation age between 5 and 15 Ma would require $\varepsilon^{182}W_{pre}$ ranging from +0.1 to −1.2, respectively. The results are shown in Fig. 3.

SUPPLEMENTARY MATERIALS

Supplementary material for this article is available at http://advances.sciencemag.org/cgi/content/full/6/7/eaay2338/DC1

Fig. S1. Localized impact melting in the martian mantle.
Fig. S2. Fate of projectile material after colliding with Mars.
Fig. S3. Details of the fate of large projectile's core clumps.
Fig. S4. Additional Hf-W isotopic evolution of early Mars.
Fig. S5. Final $\varepsilon^{182}W$ and Pt values.
References (*46*, *47*)

REFERENCES AND NOTES

1. J. M. D. Day, A. D. Brandon, R. J. Walker, Highly siderophile elements in Earth, Mars, the Moon, and Asteroids. *Rev. Mineral. Geochem.* **81**, 161–238 (2016).
2. W. F. Bottke, J. C. Andrews-Hanna, A post-accretionary lull in large impacts on early Mars. *Nat. Geosci.* **10**, 344–348 (2017).
3. R. Brasser, S. Mojzsis, A colossal impact enriched Mars' mantle with noble metals. *Geophys. Res. Lett.* **44**, 5978–5985 (2017).
4. F. Nimmo, S. D. Hart, D. G. Korycansky, C. B. Agnor, Implications of an impact origin for the martian hemispheric dichotomy. *Nature* **453**, 1220–1223 (2008).
5. M. M. Marinova, O. Aharonson, E. Asphaug, Geophysical consequences of planetary-scale impacts into a Mars-like planet. *Icarus* **211**, 960–985 (2011).
6. S. Marchi, R. M. Canup, R. J. Walker, Heterogeneous delivery of silicate and metal to the Earth by large planetesimals. *Nat. Geosci.* **11**, 77–81 (2018).
7. T. W. Dahl, D. J. Stevenson, Turbulent mixing of metal and silicate during planet accretion—And interpretation of the Hf–W chronometer. *Earth Planet. Sci. Lett.* **295**, 177–186 (2010).
8. D.-C. Lee, A. N. Halliday, Core formation on Mars and differentiated asteroids. *Nature* **388**, 854–857 (1997).
9. C. C. Reese, V. S. Solomatov, J. R. Baumgardner, Survival of impact-induced thermal anomalies in the martian mantle. *J. Geophys. Res. Planets* **107**, 5082 (2002).
10. S. Zhang, C. O'Neill, The early geodynamic evolution of Mars-type planets. *Icarus* **265**, 187–208 (2016).
11. W. S. Kiefer, Melt in the martian mantle: Shergottite formation and implications for present-day mantle convection on Mars. *Meteorit. Planet. Sci.* **38**, 1815–1832 (2003).
12. A. D. Brandon, I. S. Puchtel, R. J. Walker, J. M. D. Day, A. J. Irving, L. A. Taylor, Evolution of the martian mantle inferred from the ^{187}Re–^{187}Os isotope and highly siderophile element abundance systematics of shergottite meteorites. *Geochim. Cosmochim. Acta* **76**, 206–235 (2012).
13. T. S. Kruijer, T. Kleine, L. E. Borg, G. A. Brennecka, A. J. Irving, A. Bischoff, C. B. Agee, The early differentiation of Mars inferred from Hf-W chronometry. *Earth Planet. Sci. Lett.* **474**, 345–354 (2017).
14. S. N. Raymond, H. E. Schlichting, F. Hersant, F. Selsis, Dynamical and collisional constraints on a stochastic late veneer on the terrestrial planets. *Icarus* **226**, 671–681 (2013).
15. J. C. Andrews-Hanna, M. T. Zuber, Elliptical craters and basins on the terrestrial planets, in *Large Meteorite Impacts and Planetary Evolution IV*, R. L. Gibson, W. W. Reimold, Eds. (Special Paper 465, Geological Society of America, 2010), pp. 1–13.
16. R. M. Canup, J. Salmon, On an origin of phobos-deimos by giant impact, in *Proceedings of the 47th Lunar and Planetary Science Conference*, Woodlands, TX, 21 to 25 March 2016, p. 2598.
17. A. Ody, F. Poulet, C. Quantin, J.-P. Bibring, J. L. Bishop, M. D. Dyar, Candidates source regions of martian meteorites as identified by OMEGA/MEx. *Icarus* **258**, 366–383 (2015).
18. T. Spohn, M. H. Acuña, D. Breuer, M. Golombek, R. Greeley, A. Halliday, E. Hauber, R. Jaumann, F. Sohl, Geophysical constraints on the evolution of Mars. *Space Sci. Rev.* **96**, 231–262 (2001).

19. T. Kleine, R. J. Walker, Tungsten Isotopes in Planets. *Annu. Rev. Earth Planet. Sci.* **45**, 389–417 (2017).
20. C. N. Foley, M. Wadhwa, L. E. Borg, P. E. Janney, R. Hines, T. L. Grove, The early differentiation history of Mars from ^{182}W- ^{142}Nd isotope systematics in the SNC meteorites. *Geochim. Cosmochim. Acta* **69**, 4557–4571 (2005).
21. M. Willbold, T. Elliott, S. Moorbath, The tungsten isotopic composition of the Earth's mantle before the terminal bombardment. *Nature* **477**, 195–198 (2011).
22. H. Rizo, R. J. Walker, R. W. Carlson, M. Touboul, M. F. Horan, I. S. Puchtel, M. Boyet, M. T. Rosing, Early Earth differentiation investigated through ^{142}Nd, ^{182}W, and highly siderophile element abundances in samples from Isua, Greenland. *Geochim. Cosmochim. Acta* **175**, 319–336 (2016).
23. H. Rizo, R. J. Walker, R. W. Carlson, M. F. Horan, S. Mukhopadhyay, V. Manthos, D. Francis, M. G. Jackson, Preservation of Earth-forming events in the tungsten isotopic composition of modern flood basalts. *Science* **352**, 809–812 (2016).
24. A. Mundl, M. Touboul, M. G. Jackson, J. M. D. Day, M. D. Kurz, V. Lekic, R. T. Helz, R. J. Walker, Tungsten-182 heterogeneity in modern ocean island basalts. *Science* **356**, 66–69 (2017).
25. N. Dauphas, A. Pourmand, Hf-W-Th evidence for rapid growth of Mars and its status as a planetary embryo. *Nature* **473**, 489–492 (2011).
26. R. Morishima, G. J. Golabek, H. Samuel, N-body simulations of oligarchic growth of Mars: Implications for Hf-W chronology. *Earth Planet. Sci. Lett.* **366**, 6–16 (2013).
27. M. S. Clement, N. A. Kaib, S. N. Raymond, K. J. Walsh, Mars' growth stunted by an early giant planet instability. *Icarus* **311**, 340–356 (2018).
28. L. C. Bouvier, M. M. Costa, J. N. Connelly, N. K. Jensen, D. Wielandt, M. Storey, A. A. Nemchin, M. J. Whitehouse, J. F. Snape, J. J. Bellucci, F. Moynier, A. Agranier, B. Gueguen, M. Schönbächler, M. Bizzarro, Evidence for extremely rapid magma ocean crystallization and crust formation on Mars. *Nature* **558**, 568–589 (2018).
29. H. F. Levison, K. A. Kretke, K. J. Walsh, W. F. Bottke, Growing the terrestrial planets from the gradual accumulation of submeter-sized objects. *Proc. Natl. Acad. Sci. U.S.A.* **112**, 14180–14185 (2015).
30. K. Mezger, V. Debaille, T. Kleine, Core formation and mantle differentiation on Mars. *Space Sci. Rev.* **174**, 27–48 (2013).
31. H. Wang, B. P. Weiss, X.-N. Bai, B. G. Downey, J. Wang, J. Wang, C. Suavet, R. R. Fu, M. E. Zucolotto, Lifetime of the solar nebula constrained by meteorite paleomagnetism. *Science* **355**, 623–627 (2017).
32. J. Bollard, J. N. Connelly, M. Bizzarro, Pb-Pb dating of individual chondrules from the CB_a chondrite Gujba: Assessment of the impact plume formation model. *Meteorit. Planet. Sci.* **50**, 1197–1216 (2015).
33. J. D. Kendall, H. J. Melosh, Differentiated planetesimal impacts into a terrestrial magma ocean: Fate of the iron core. *Earth Planet. Sci. Lett.* **448**, 24–33 (2016).
34. H. Genda, R. Brasser, S. J. Mojzsis, The terrestrial late veneer from core disruption of a lunar-sized impactor. *Earth Planet. Sci. Lett.* **480**, 25–32 (2017).
35. M. Jutzi, SPH calculations of asteroid disruptions: The role of pressure dependent failure models. *Planet. Space Sci.* **107**, 3–9 (2015).
36. L. E. Senft, S. T. Stewart, Dynamic fault weakening and the formation of large impact craters. *Earth Planet. Sci. Lett.* **287**, 471–482 (2009).
37. S. E. Smrekar, P. Lognonné, T. Spohn, W. B. Banerdt, D. Breuer, U. Christensen, V. Dehant, M. Drilleau, W. Folkner, N. Fuji, R. F. Garcia, D. Giardini, M. Golombek, M. Grott, T. Gudkova, C. Johnson, A. Khan, B. Langlais, A. Mittelholz, A. Mocquet, R. Myhill, M. Panning, C. Perrin, T. Pike, A.-C. Plesa, A. Rivoldini, H. Samuel, S. C. Stähler, M. van Driel, T. Van Hoolst, O. Verhoeven, R. Weber, M. Wieczorek, Pre-mission InSights on the interior of Mars. *Space Sci. Rev.* **215**, 3 (2019).
38. A. Emsenhuber, M. Jutzi, W. Benz, SPH calculations of Mars-scale collisions: The role of the equation of state, material rheologies, and numerical effects. *Icarus* **301**, 247–257 (2018).
39. B. A. Ivanov, H. J. Melosh, E. Pierazzo, Basin-forming impacts: Reconnaissance modeling, in *Large Meteorite Impacts and Planetary Evolution IV*, R. L. Gibson, W. U. Reimold, Eds. (Geological Society of America, 2010), vol. 465.
40. G. S. Collins, H. J. Melosh, B. A. Ivanov, Modeling damage and deformation in impact simulations. *Meteorit. Planet. Sci.* **39**, 217–231 (2004).
41. H. J. Melosh, *Impact Cratering: A Geologic Process* (Oxford Univ. Press, 1989).
42. N. L. Chabot, H. Haack, *Evolution of Asteroidal Cores*, D. S. Lauretta, H. Y. McSween, Eds. (University of Arizona Press, 2006), pp. 747–771.
43. E. Cottrell, M. J. Walter, D. Walker, Metal-silicate partition of tungsten at high pressure and temperature:Implications for equilibrium core formation in Earth. *Earth Planet. Sci. Lett.* **281**, 275–287 (2009).
44. A. Morbidelli, D. Nesvorny, V. Laurenz, S. Marchi, D. C. Rubie, L. Elkins-Tanton, M. Wieczorek, S. Jacobson, The timeline of the lunar bombardment: Revisited. *Icarus* **305**, 262–276 (2018).
45. S. Marchi, W. F. Bottke, L. T. Elkins-Tanton, M. Bierhaus, K. Wuennemann, A. Morbidelli, D. A. Kring, Widespread mixing and burial of Earth's Hadean crust by asteroid impacts. *Nature* **511**, 578–582 (2014).
46. R. G. Kraus, S. Root, R. W. Lemke, S. T. Stewart, S. B. Jacobsen, T. R. Mattsson, Impact vaporization of planetesimal cores in the late stages of planet formation. *Nat. Geosci.* **8**, 269–272 (2015).
47. J. M. Y. Woo, H. Genda, R. Brasser, S. J. Mojzsis, Mars in the aftermath of a colossal impact. *Icarus* **333**, 87–95 (2019).

Acknowledgments: We thank M. Jutzi, P. Michel, and E. Asphaug for useful discussions about SPH methods. We also thank K. Pahlevan and T. Kleine for constructive comments. **Funding:** This study was supported by NASA Habitable Worlds grant NNX16AR87G and NASA SSERVI grant NNA14AB07A. **Author contributions:** S.M. conceived the work and carried out analysis of SPH simulation outputs and isotopic mixing calculations. R.J.W. guided the execution of isotopic calculations, and R.M.C. executed the SPH simulations. All participated in the writing of the manuscript and discussion of the results. **Competing interests:** The authors declare that they have no competing interests. **Data and materials availability:** All data needed to evaluate the conclusions in the paper are present in the paper and the Supplementary Materials. Selected SPH and isotopic mixing outputs are available upon request.

Submitted 31 May 2019
Accepted 26 November 2019
Published 12 February 2020
10.1126/sciadv.aay2338

Citation: S. Marchi, R. J. Walker, R. M. Canup, A compositionally heterogeneous martian mantle due to late accretion. *Sci. Adv.* **6**, eaay2338 (2020).